Optical Properties of a Nanoegg-Nanorod Heterodimer: A Quasi-Static Analysis

Luke C. Ugwuoke,[1] Tomáš Mančal,[2] and Tjaart P. J. Krüger[1]

[1)]*Department of Physics, University of Pretoria.*

Private bag X20, Hatfield 0028, South Africa[a)]

[2)]*Faculty of Mathematics and Physics, Charles University.*

Ke Karlovu 5, 121 16 Prague 2, Czech Republic

(Dated: 3 August 2020)

Plasmon coupling between the dipolar localized surface plasmons of a nanoegg and the longitudinal dipolar localized surface plasmons of a nearby gold nanorod is investigated within a dipolar-quasistatic limit. This was achieved by varying the core-offset of the nanoegg for different nanorod sizes at a fixed coupling distance. With respect to the plasmon peaks of the isolated nanoegg, we studied blueshifted, resonant, and redshifted nanorods. We show that besides plasmon-induced resonance shifts, which occurred in all three cases studied, transparency dips are induced in both the absorption and scattering spectra of the nanoegg-nanorod dimer. The latter effect depends on the plasmon detuning frequency and the nanorod absorption cross-section. In comparison to a nanoegg-nanosphere dimer, the optical properties of the nanoegg-nanorod dimer are more enhanced.

Keywords: Electrostatic polarizability, Localized surface plasmon resonance, Nanoegg, Nanorod, Plasmon coupling, Plasmon-Induced transparency

I. INTRODUCTION

Particle-confined oscillations of conduction electrons, due to their collective harmonic motion upon resonant excitation of surface plasmon modes of a metal nanoparticle (MNP), result in localized surface plasmon resonance (LSPR)[1,2]. Asymmetric metal–dielectric nanostructures such as nanoeggs[1–5] possess great LSPR tunability due to their ability to support the plasmon hybridization of cavity and solid plasmons with both different and the same angular momentum numbers[1,2]. Engineered primarily by off-setting the core of a concentric nanoshell, this symmetry-breaking property of nanoeggs enables the manifestation of dipole-active modes[3,4] in their extinction spectra. In addition, a typical nanoegg (NE) absorption spectrum, based on the two lowest-order plasmonic modes (the dipole and the quadrupole modes), features a Fano dip[5], also known as a plasmon-induced trans-

[a)]Electronic mail: luke.ugwuoke@up.ac.za, tjaart.kruger@up.ac.za

parency (PIT) dip[6,7]. This is a region of reduced or zero absorption as a result of dipole–quadrupole plasmon coupling[5].

Likewise, the aspect ratio of a nanorod (NR) enables its LSPR to be tuned with great sensitivity along the longitudinal axis[8–15]. Both the longitudinal dipolar LSPR of a NR[8,14–18] and the dipolar LSPR of a NE[4,5] have a common property, namely a redshift in their LSPR with an increase in their respective asymmetry parameters, i.e., the aspect ratio of the NR and the core-offset of the NE. When these two nanoparticles are spatially separated by a small gap, a NE-NR heterodimer is formed. Although nanoeggs are more complicated to synthesize than concentric nanoshells, they can be fabricated, as demonstrated in Refs.[1,2]. Thus, the proposed dimer is practically realistic. A heterodimer similar to the one proposed here, where a gold nanosphere (NS) was used to modify the optical spectra of a gold NR, was studied in Ref.[7]. The optical properties of nanoparticle dimers, such as NS dimers[19–23], NR dimers[23–25], concentric nanoshell dimers[26,27], NS-concentric nanoshell dimers[28,29], pairs of cavity resonance based plasmonic nanoantennas[30], and nanowire dimers[31–33] have been widely studied in plasmonic literature. While significantly more strongly enhanced near-fields have been reported to exist in dimer gaps[19,27,34,35], the spectra of dimers also differ from those of single nanoparticles, predominantly because they feature incident electric field polarization-dependent response, plasmon-induced resonance shifts, and PIT regions[21,24,28].

Major applications of the different plasmonic behaviour in these nanostructures range from photocurrent enhancement in bio-hybrid solar cells[36–38], enhancement of Raman signals in surface-enhanced Raman spectroscopy[39], plasmon-enhanced fluorescence in emitter–MNP systems[40–45], to refractive index sensing in plasmonic systems[4,46]. PIT is also a form of electromagnetically-induced transparency (EIT)[6,23,47], a mechanism that can be used to slow, stop, or store light[48]. It has also been shown that plexcitonic systems exhibit EIT[49**?** ,50] due to the interaction between excitonic resonances of molecular aggregates[50,51] and LSPR of metallic nanostructures[18,49,52].

The aim of this study is to investigate the effect of plasmon coupling on the optical properties of a NE-NR heterodimer as the longitudinal LSPR of the NR is tuned via its size. We chose to study a NE since, unlike the concentric nanoshell, the LSPR of a NE can be tuned at constant particle size via its core-offset[1,2]. We studied small nanorods to ensure that only dipolar NR plasmons, which can be fully described via a quasi-static approach, are considered. Likewise, radiation broadening of the scattering and absorption spectra[12,18,23,33], due to radiation of incident light as the particle sizes become comparable to the wavelength of light in the medium, is avoided. The optical properties studied in this work include the effective scattering and absorption spectra of the NE-NR dimer, as well as the characteristics of such hybrid spectra. We approximated the NR to a solid prolate spheroid, a usual practice in analytical models[52]. A uniform electric field, parallel to the dimer axis, polarizes the NR along its long axis in the direction of the core-offset of the NE, as shown in Fig. 1. An incident field perpendicular to the dimer axis will polarize the NR along its short axis and the NE across its core-offset. Since these transverse LSPRs have poor tunabilities compared to their

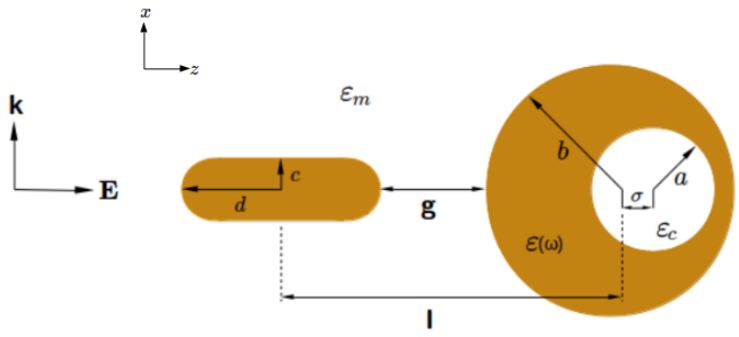

FIG. 1. Model geometry of the nanoegg–nanorod dimer. The dimer is surrounded by a homogeneous dielectric medium of dielectric constant ε_m. The NR is modelled as a prolate gold spheroid in the presence of a uniform electric field **E** polarized in the z-direction, with a propagation wavevector **k** in the x-direction. The NE consists of a gold shell of dielectric constant $\varepsilon(\omega)$, an off-centre silica core of dielectric constant ε_c, and a core-offset σ, in the positive z-direction. The surface-to-surface distance is $\mathbf{g} = g\hat{z}$, and the centre-to-centre distance is $\mathbf{l} = l\hat{z}$.

longitudinal counterparts[1,2,8,18], this incident field direction will not be considered.

II. THEORY

The scattering problem of a NE in an external electric field has been solved by Norton and Vo-Dinh[5] using a quasi-static approach. However, an explicit expression for the static polarizability was not obtained. In Section II A, we will obtain the static dipole polarizability of the NE, based on the two lowest-order plasmonic modes. In Section II B, we will obtain an effective static dipole polarizability of the NE-NR dimer using a dipolar quasi-static approach[29,52,53].

A. Nanoegg in a Uniform Electrostatic Field

The solution of the Laplace equation in spherical coordinates for the potentials in the core region, the shell region, and in the medium outside the NE, for an incident field polarized in the z-direction, are represented, respectively, as[5]:

$$\Phi_c(r_c,\theta_c) = \sum_{n=1}^{\infty} A_n \left(\frac{r_c}{a}\right)^n P_n(\cos\theta_c), \tag{1}$$

$$\Phi_s(r_s,\theta_s) = \sum_{n=1}^{\infty} \left[B_n \left(\frac{r_s}{b}\right)^n + C_n \left(\frac{b}{r_s}\right)^{n+1}\right] P_n(\cos\theta_s), \tag{2}$$

$$\Phi_m(r_s,\theta_s) = \Phi_{inc}(r_s,\theta_s) + \Phi_{sca}(r_s,\theta_s), \tag{3}$$

where

$$\Phi_{inc}(r_s,\theta_s) = E_n\Big(\frac{r_s}{b}\Big)^n P_n(\cos\theta_s), \quad E_n = \begin{cases} -E_0 b, & n=1 \quad \text{(Bright mode)} \\ 0, & n\geq 2 \quad \text{(Dark modes)} \end{cases}, \tag{4}$$

is the incident potential, and

$$\Phi_{sca}(r_s,\theta_s) = \sum_{n=1}^{\infty} D_n\Big(\frac{b}{r_s}\Big)^{n+1} P_n(\cos\theta_s) \tag{5}$$

is the scattered potential. Here, r_c and r_s, the radial coordinates of the core and shell, respectively, have been normalized with their respective values at the interfaces. The function $P_n(\cos\theta)$ is the Legendre function of the first kind, A_n, B_n and C_n, and D_n are the complex amplitudes of the electrostatic potential in the core, shell, medium regions, respectively, and E_n is the amplitude of the incident potential.

To obtain the static dipole polarizability, we need to express D_1 in terms of E_0. In Ref.[45], a similar problem was solved using a point dipole field as the incident field source, where a quasi-static multipole polarizability of the NE was obtained. Here, we adopt the same approach but with the dipole potential replaced with the external potential given by Eq. 4. In this approach, the boundary conditions are applied at the shell–medium and core–shell boundaries, the solid-harmonic addition theorem[54] is applied at the core–shell boundary, the orthogonality property of the Legendre polynomial of the first kind is considered, using Eq. 4 instead of Eq. (5) of Ref.[45], and D_1 is finally solved using the resulting equations based on the two lowest-order modes, $n=1$ and $n=2$, in Appendix A of Ref.[45], to obtain

$$D_1 = \left[\frac{9\varepsilon(\omega)\varepsilon_m K_{11}\Big(\varepsilon_c-\varepsilon(\omega)\Big)\kappa_2 + \Big(\varepsilon(\omega)-\varepsilon_m\Big)\Big(\kappa_1\kappa_2-\kappa_3\Big)}{\Big(\varepsilon(\omega)+2\varepsilon_m\Big)\Big(\kappa_1\kappa_2-\kappa_3\Big)}\right] E_0 b, \tag{6}$$

where

$$\kappa_0 = \Big(\varepsilon_c-\varepsilon(\omega)\Big)\Big(\varepsilon(\omega)-\varepsilon_m\Big), \tag{7}$$

$$\kappa_1 = 2K_{11}\kappa_0 + M_{11}\Big(\varepsilon_c+2\varepsilon(\omega)\Big)\Big(2\varepsilon_m+\varepsilon(\omega)\Big), \tag{8}$$

$$\kappa_2 = 6K_{22}\kappa_0 + M_{22}\Big(2\varepsilon_c+3\varepsilon(\omega)\Big)\Big(3\varepsilon_m+2\varepsilon(\omega)\Big), \tag{9}$$

$$\kappa_3 = 3K_{12}M_{21}\kappa_0\Big(\varepsilon(\omega)+2\varepsilon_m\Big)\Big(3\varepsilon(\omega)+2\varepsilon_c\Big), \tag{10}$$

and

$$K_{11} = \Big(\frac{a}{b}\Big), K_{22} = \Big(\frac{a}{b}\Big)^2, M_{11} = \Big(\frac{b}{a}\Big)^2, M_{22} = \Big(\frac{b}{a}\Big)^3, \tag{11}$$

$$K_{12} = 2\Big(\frac{a}{b^2}\Big)\sigma, M_{21} = -2\Big(\frac{b^2}{a^3}\Big)\sigma. \tag{12}$$

Here, K_{11} and M_{11} are coupling constants of solid and cavity dipole sphere plasmons, respectively, K_{22} and M_{22} are coupling constants of solid and cavity quadrupole sphere plasmons, respectively,

and K_{12} and M_{21} are the dipole–quadrupole and quadrupole–dipole coupling constants of solid and cavity sphere plasmons, respectively.

Next, we evaluate Eq. (5) for $n = 1$ and compare the result to the potential of a point dipole in a medium of dielectric constant ε_m[9,40] to obtain the static dipole polarizability of the NE as

$$\alpha_{NE} = 4\pi b^2 \frac{D_1}{E_0}. \tag{13}$$

B. Nanoegg Coupled to a Small Nanorod

The optical response of a NE near a NR can be investigated using a dipolar quasi-static approach, provided that the nanoparticle sizes and the inter-particle distance are small compared to the wavelength of light in the medium[9,29,52,53]. This allows one to ignore radiation damping, the spatial variation of the incident electric field, and the wavenumber-dependent terms in the induced field on each particle[29,53]. This approach has been shown to agree with experiments involving small nanoparticles less than 30 nm in radius[29,33]. Beyond such sizes, the quasi-static model is not valid[9,33]. The method also requires that the nanoparticles are such that the probability of electrons tunnelling through the dimer gap is zero. Esteban et al.[19] have shown that the probability for quantum tunnelling is negligible in dimer gaps greater than or equal to 0.5 nm, so that classical methods are valid in this regime. In addition, the local electric field, $\mathbf{E}_{loc}$, on each nanoparticle in the dimer is represented as that of an induced electric dipole, $\mathbf{E}_{ind}$, at the centre of the other particle, and the external field, $\mathbf{E}_0$, applied to the dimer[29,53].

For the NE-NR dimer, with $\mathbf{E}_0$ parallel to the dimer axis, as shown in Fig. 1, we write the parallel components of the local fields as:

$$E_{loc}^{NR} = E_0 + E_{ind}^{NE}, \tag{14}$$

$$E_{loc}^{NE} = E_0 + E_{ind}^{NR}, \tag{15}$$

where

$$E_{ind}^{NE} = \frac{P_{NE}}{2\pi\varepsilon_m l^3}, \tag{16}$$

$$P_{NE} = \alpha_{NE}\varepsilon_m E_{loc}^{NE} = \alpha_{NE}^{eff}\varepsilon_m E_0, \tag{17}$$

and[18,40]

$$E_{ind}^{NR} = \frac{3P_{NR}[1-L(v_2)]}{4\pi\varepsilon_m l(l^2-f^2)}, \;\; l = d+g+b, \tag{18}$$

$$P_{NR} = \alpha_{NR}\varepsilon_m E_{loc}^{NR} = \alpha_{NR}^{eff}\varepsilon_m E_0, \tag{19}$$

with[9,18]

$$L(v_i) = (v_i^2-1)[(v_i \coth^{-1} v_i) - 1], \;\; i = 1,2, \tag{20}$$

$$v_1 = (1-q^{-2})^{-\frac{1}{2}}, \;\; v_2 = l/f, \;\; q = d/c, \;\; f = \sqrt{d^2-c^2}, \tag{21}$$

$$\alpha_{NR} = \frac{4\pi dc^2}{3}\left[\frac{\varepsilon(\omega)-\varepsilon_m}{\varepsilon_m + L(v_1)[\varepsilon(\omega)-\varepsilon_m]}\right]. \tag{22}$$

Here, E_{ind}^{NE} is the induced spherical dipole field due to the NE, E_{ind}^{NR} is the induced spheroidal dipole field due to the NR, P_{NE} and P_{NR} are dipole moments of the NE and NR, respectively, α_{NR} is the longitudinal static dipole polarizability of the NR, v_1 and v_2 are the radial coordinates of the NR and the NE-NR system, respectively, $L(v_1)$ and $L(v_2)$ are the the longitudinal static geometric factors of the NR and the NE-NR system, respectively, q is the aspect ratio of the NR, f is the focal distance of the NR, and α_{NE}^{eff} and α_{NR}^{eff} are the effective dipole polarizabilities of the NE and NR, respectively.

By substituting Eq. (16) into Eq. (14), Eq. (14) into Eq. (19), and Eq. (19) into Eq. (18), followed by substituting Eq. (18) into Eq. (15), and making use of Eq. (17), we obtain

$$\alpha_{NE}^{eff} = \alpha_{NE}\left[1+\frac{3\alpha_{NR}[1-L(v_2)]}{4\pi l(l^2-f^2)}\right]\left[1-\frac{3\alpha_{NR}\alpha_{NE}[1-L(v_2)]}{2(2\pi l^2)^2(l^2-f^2)}\right]^{-1}. \tag{23}$$

Similarly, by substituting Eq. (18) into Eq. (15), Eq. (15) into Eq. (17), and Eq. (17) into Eq. (16), followed by substituting Eq. (16) into Eq. (14), and making use of Eq. (19), we obtain

$$\alpha_{NR}^{eff} = \alpha_{NR}\left[1+\frac{\alpha_{NE}}{2\pi l^3}\right]\left[1-\frac{3\alpha_{NR}\alpha_{NE}[1-L(v_2)]}{2(2\pi l^2)^2(l^2-f^2)}\right]^{-1}. \tag{24}$$

The quasi-static dipole polarizability of the dimer is calculated as

$$\alpha = \alpha_{NR}^{eff} + \alpha_{NE}^{eff}. \tag{25}$$

In the quasi-static limit, the scattering and absorption cross-sections of the dimer can be calculated using[9,29]

$$C_{sca} = \frac{k^4}{6\pi}|\alpha|^2, \quad \text{and} \quad C_{abs} = k\Im[\alpha], \tag{26}$$

respectively. Here, $k = 2\pi\sqrt{\varepsilon_m}/\lambda$ is the wavenumber of light in the medium.

We will use the following Lorentz–Drude local dielectric function for gold[55]:

$$\varepsilon(\omega) = \varepsilon_\infty - \frac{s\omega_b^2}{\omega(\omega+i\gamma_b)-\omega_b^2} - \frac{\omega_f^2}{\omega(\omega+i\gamma_f)}. \tag{27}$$

It agrees with experimental data in the region $\omega = 1.24$ eV to $\omega = 2.48$ eV, with model parameters $\varepsilon_\infty = 5.9673$, $\omega_b = 2.6885$ eV, $\gamma_b = 0.4337$ eV, $\omega_f = 8.7411$ eV, $\gamma_f = 0.0658$ eV, and $s = 1.09$. Here, ε_∞ is the high-frequency dielectric constant of gold, which accounts for the polarization of the positive ion core, γ_b and ω_b are the damping rate and resonance frequency of the bound electrons, respectively, s is the oscillator strength, γ_f and ω_f are the damping rate and plasma frequency of the free electrons, respectively, and ω is the photon energy. We will use Eq. 27 to represent the dielectric function of both the gold shell and the gold NR. In addition, $\varepsilon_c = 2.13$[1] is used as the dielectric constant of the silica core, and water, with a dielectric constant of $\varepsilon_m = 1.77$, is used as the medium.

III. RESULTS AND DISCUSSION

We will consider a NE with dimensions $a = 15$ nm and $b = 20$ nm, and the following core-offsets: $\sigma = 0.0, 1.0, 2.0, 3.0$, and 4.0 nm. For a given aspect ratio of the NR, the dipolar LSPR of the NE

is tuned via its core-offset to make it resonant or off-resonant with the longitudinal dipolar LSPR of the NR, while the coupling distance is kept constant. The dimer gap, g, will be set to 1.0 nm, a typical gap distance that has been reported experimentally for heterodimers in aqueous solutions[7]. Likewise, Eqs. (23) and (24) show that the plasmon coupling terms, which are proportional to $3\alpha_{NR}\alpha_{NE}[1-L(v_2)]/4\pi l(l^2-f^2)$, and $\alpha_{NR}\alpha_{NE}/2\pi l^3$, respectively, are strongly dependent on short dimer gaps. Since each of the coupling terms is proportional to α_{NR}/l at constant g and α_{NE}, we will consider several nanorods with different α_{NR} by varying both c and d in order to tune the plasmon coupling strength.

A. Absorption and Scattering Spectra of the Dimer

As shown in Fig. 2(**a**), the dipolar LSPR of the NE, which we denote as ω_{ne}, undergoes a redshift with increasing core-offset, i.e., from $\omega_{ne} = 615$ nm when $\sigma = 0.0$ nm to $\omega_{ne} = 652$ nm when $\sigma = 4.0$ nm, in agreement with Ref.[5]. At large core-offsets, a quadrupole LSPR is also noticeable in Fig. 2(**a**) at around 550 nm, due to an increase in the dipole–quadrupole plasmon coupling strength. In the NE-NR dimer, we studied two groups of NR sizes. For the big nanorods, their absorption cross-sections are comparable to those of the isolated NE, i.e., the NR sizes (d,c) are (24 nm, 12 nm), (24 nm, 9.6 nm), and (24 nm, 8 nm), as shown in panel 1 of Fig. 2(**b**), while for the small nanorods, their absorption cross-sections are small compared to those of the isolated NE, i.e., the NR half-length and half-width, (d,c), are (15 nm, 7.5 nm), (15 nm, 6 nm), and (15 nm, 5 nm), as shown in panel 2 of Fig. 2(**b**). In the quasi-static limit, the dipolar plasmon resonances of the different NR sizes, which we denote as ω_{nr}, are the same when they have the same aspect ratio[12,18], i.e., $\omega_{nr} = 586$ nm, 625 nm, and 673 nm, corresponding to q = 2.0, 2.5 and 3.0, respectively, while their absorption cross-sections are different, as shown in Fig. 2(**b**), panels 1 and 2, respectively). The absorption spectra of the NE-NR dimer are shown in Fig. 3 while the scattering spectra are shown in Fig. 4 for each of the three plasmon peak positions of the nanorods with respect to those of the NE, respectively.

For the blueshifted nanorods i.e., the nanorods with half-dimensions (24 nm, 12 nm) and (15 nm, 7.5 nm), with a LSPR of 586 nm, the absorption and scattering spectra of the NE-NR dimer in Figs. 3((**a**), (**d**)) and 4((**a**), (**d**)), respectively, show a gradual appearance of transparency dips and mode splittings as ω_{ne} redshifts from ω_{nr}. This is due to an increase in the plasmon detuning frequency, $\omega_{ne} - \omega_{nr}$, which leads to mode splitting. However, the big NR, with half-dimensions (24 nm, 12 nm), whose plasmon linewidth and absorption cross-section are comparable to those of the NE (Fig. 2), induces more plasmon shifts and some noticeable transparency dips, and leads to more enhanced spectra, as shown in Figs. 3(**a**) and 4(**a**), due to its large absorption cross-section (Fig. 2(**b**), panel 1) compared to that of the small NR with dimensions (15 nm, 7.5 nm) (Fig. 2(**b**), panel 2). For the small NR, nearly only plasmon-induced LSPR shifts occur in the dimer spectra in

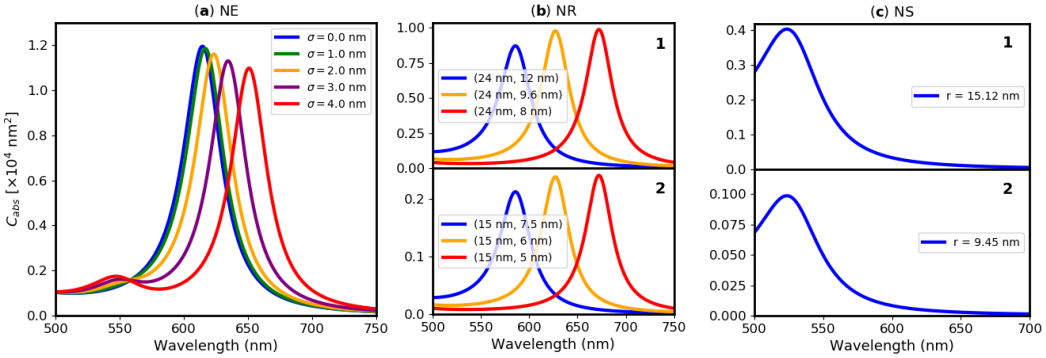

FIG. 2. Absorption cross-sections of the uncoupled nanoparticles. (**a**) Absorption cross-sections of the NE for each of the core-offsets studied. (**b**) Absorption cross-sections of the big nanorods (panel **1**) and those of the small nanorods (panel **2**), respectively. (**c**) Absorption cross-section of a nanosphere with the same volume as that of the blueshifted big NR (panel **1**) and small NR (panel **2**).

Figs. 3(**d**) and 4(**d**), even when the detuning frequency is high. This is because the NR absorption cross-section (Fig. 2(**b**), panel 2) is too small compared to those of the NE (Fig. 2(**a**)). In addition, the plasmon-induced shifts in the spectra of the NE-NR dimer, i.e., the strong redshifts in ω_{ne} and the weak blueshifts in ω_{nr}, are slightly more for the big NR due to its large polarizability.

Figs. 3(**b**) and 4(**b**) show the absorption and scattering spectra of the dimer when the NE is coupled to a big NR, (24 nm, 9.6 nm), with $\omega_{nr} = 625$ nm resonant with the NE at $\sigma = 2.0$ nm, whose absorption cross-section is comparable to that of the NE (Fig. 2(**b**), panel 1). The spectra of the NE-NR dimer (Figs. 3(**b**) and 4(**b**)) only feature plasmon-induced LSPR shifts. This is because the plasmon coupling strength is small, since a long half-length of the NR leads to a longer inter-particle distance, so that plasmon hybridization leads only to a strong redshift in ω_{ne}, even beyond zero detuning ($\omega_{ne} \neq \omega_{nr}$). In addition, the plasmon linewidths of the isolated NE and NR absorption spectra are comparable (Fig. 2(**a**) and Fig. 2(**b**), panel 1), so that Fano interference does not occur. However, when the NE is coupled to a small NR, (15 nm, 6 nm), whose absorption cross-section is smaller than that of the NE, and also resonant with the NE at $\sigma = 2.0$ nm (Fig. 2(**b**), panel 2), both the scattering and absorption spectra of the dimer feature some noticeable induced transparency when $\sigma \leq 2.0$ nm (Figs. 3(**e**) and 4(**e**)). In this case, the plasmon linewidths of the isolated NE and NR are not comparable and the coupling strength due to the (15 nm, 6 nm) NR is more than that of the (24 nm, 9.6 nm) NR as a result of its short half-length, so that Fano interference can occur, but plasmon hybridization only leads to mode splitting when $\sigma \leq 2.0$ nm. Beyond $\sigma = 2.0$ nm, the NR absorption is too small compared to that of the NE for any significant mode splitting to take place. Similar to the blueshifted NR case, the plasmon-induced LSPR shifts are slightly greater and the spectra of the dimer are more enhanced when the NR is bigger due to its large polarizability.

In the case of redshifted nanorods, the absorption and scattering spectra of the NE-NR dimer in

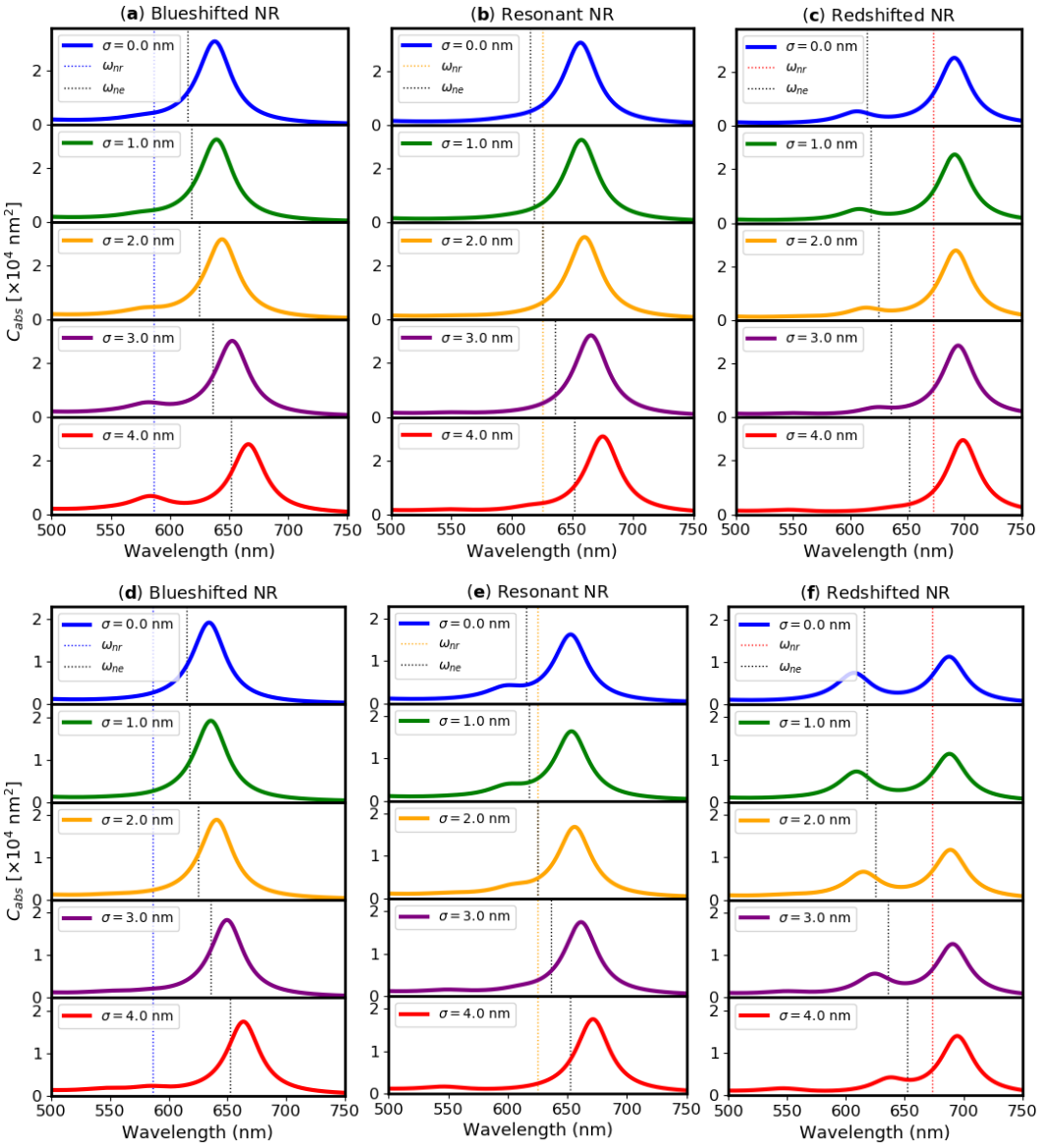

FIG. 3. Absorption cross-sections of the NE-NR dimer, for the different core-offsets of the NE, in the case of nanorods with different absorption cross-sections and plasmon peak positions, corresponding to NR sizes (d, c): (**a**) (24 nm, 12 nm) NR and (**d**) (15 nm, 7.5 nm) NR (Blueshifted nanorods), (**b**) (24 nm, 9.6 nm) NR and (**e**) (15 nm, 6 nm) NR (Resonant nanorods), and (**c**) (24 nm, 8 nm) NR and (**f**) (15 nm, 5 nm) NR (Redshifted nanorods), with respect to those of the NE. Top row: the big nanorods. Bottom row: the small nanorods. The dotted lines represent the plasmon peak positions of the NR and NE, respectively.

Figs. 3(**c**) and 4(**f**), respectively, show a gradual decrease in both the induced transparency dips and mode splittings as ω_{ne} approaches ω_{nr}. This is expected since the detuning frequency, $\omega_{nr} - \omega_{ne}$, decreases in this case so that mode splitting becomes more unlikely. However, the small NR, (15 nm, 5 nm), induces significant transparency dips in the dimer spectra (Figs. 3(**f**) and 4(**f**)) compared

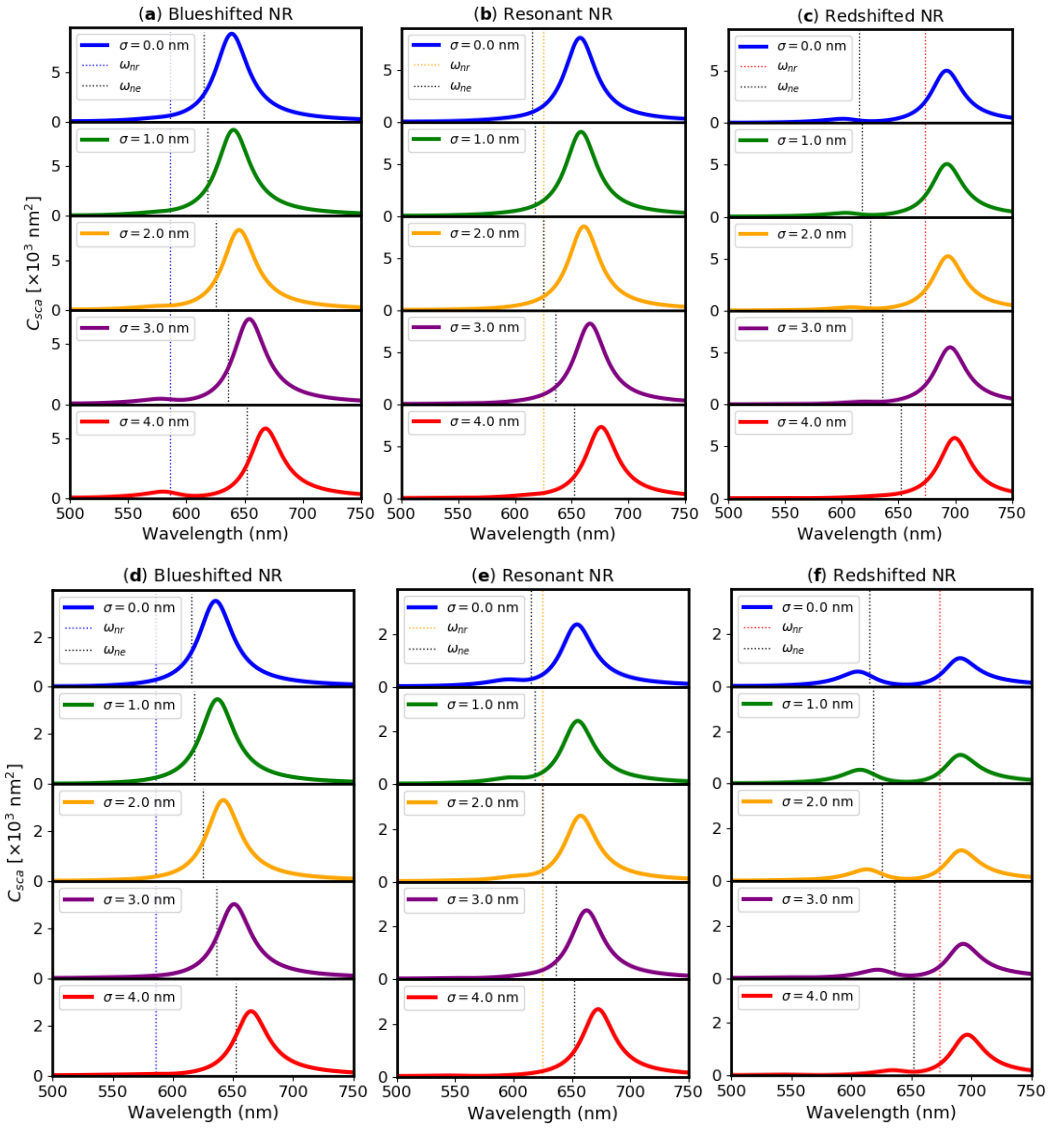

FIG. 4. Scattering cross-sections of the NE-NR dimer, for the different core-offsets of the NE, in the case of nanorods with different absorption cross-sections and plasmon peak positions, corresponding to NR sizes (d, c): (**a**) (24 nm, 12 nm) NR and (**d**) (15 nm, 7.5 nm) NR (Blueshifted nanorods), (**b**) (24 nm, 9.6 nm) NR and (**e**) (15 nm, 6 nm) NR (Resonant nanorods), and (**c**) (24 nm, 8 nm) NR and (**f**) (15 nm, 5 nm) NR (Redshifted nanorods), with respect to those of the NE. Top row: the big nanorods. Bottom row: the small nanorods. The dotted lines represent the plasmon peak positions of the NR and NE, respectively.

to the dimer spectra for the big NR, (24 nm, 8 nm) (Figs. 3(**c**) and 4(**c**)), irrespective of the detuning frequency. As a result, the smaller NR can enhance or reduce the cross-sections of the NE-NR dimer (Figs. 3(**f**) and 4(**f**)) depending on the core-offset of the NE. This is partly due to the difference between the plasmon linewidths of the isolated NE (Fig. 2(**a**)) and the small NR (Fig. 2(**b**, panel 2) compared to that of the big NR (Fig. 2(**b**, panel 1), and also due to a stronger coupling strength in

the dimer when the NR half-length is short due to a smaller centre-to-centre distance. The plasmon-induced shifts in the dimer spectra, i.e., the weak redshifts in ω_{nr} and the strong blueshifts in ω_{ne}, and the enhancement of the cross-sections for the big NR are greater than those of the small NR due to the large polarizability of the former. Similar size-dependent spectral shifts and enhancement of optical cross-sections have been reported for other dimers studied in Refs.[7,28,29]. For instance, similar to one of the scattering spectra of the NS-NR dimer studied in Ref.[7], when the NS is located at the end of the NR and the NR is at a redshifted plasmon peak position with respect to the plasmon peak of the NS, the scattering spectra of the NE-NR dimer (Fig. 4(**f**)) also contain two scattering peaks. However, for the NE-NR dimer, a high-energy peak, which is weak and decreases with increasing core-offset, and a low-energy peak, which is strong and increases with decreasing core-offset, are formed.

When $\sigma = 0.0$ nm, i.e., a concentric nanoshell, the transparency dips in both the absorption and scattering spectra of the NE-NR dimer (Fig. 3 and Fig. 4) are more noticeable in the redshifted small NR case (Fig. 3(**f**) and Fig. 4(**f**, top panels) compared to those of the blueshifted small NR case (Fig. 3(**d**) and Fig. 4(**d**, top panels), whereas at large core-offsets, such as $\sigma = 4.0$ nm, the converse is true for the big nanorods (Fig. 3(**a**) and Fig. 4(**a**, bottom panels). Again, this behaviour is due to the detuning frequency, which can be increased or decreased with respect to the spectral peak position of the NR.

We considered nanospheres with the same volume as the blueshifted nanorods by using the equivalent sphere-volume radius of the NR as the radius of the NS in each case, i.e., $r = \sqrt[3]{dc^2}$, to obtain $r = 15.12$ nm for the (24 nm, 12 nm) NE-NR dimer and $r = 9.45$ nm for the (15 nm, 7.5 nm) NE-NR dimer. Their dipolar LSPR, which is at around 525 nm, as shown in Fig. 2(**c**, panels 1 and 2), is the same in the quasi-static limit. To obtain the polarizability of the NE-NS dimer from that of NE-NR dimer, we set $L(v_1) = L(v_2) = 1/3$, i.e., the static geometric factor of an isotropic sphere[12,18], $f = 0$, and $l = r + g + b$. As shown in Fig. 5, both the absorption and scattering spectra of the NE-NS dimer are less enhanced compared to those of the NE-NR dimer (Figs. 3(**a**)-(**f**) and 4(**a**)-(**f**), respectively), for the blueshifted NR case. This is due to the smaller polarizability of the NS compared to that of the NR of the same volume. Compared to the NE-NR dimer, the spectra of the NE-NS dimer (Fig. 5) are dominated by plasmon-induced LSPR shifts due to the small absorption cross-section of the NS compared to that of the NE. However, the trends that lead to plasmon-induced shifts and induced transparency in the NE-NS dimer are similar to those of the NE-NR dimer for the blueshifted NR case.

In the above discussions, we have attributed the plasmon-induced transparency phenomenon to either plasmon hybridization or Fano interference or both, since the plasmon linewidths of the dipolar modes of the NR and the NE can be comparable or are dissimilar, depending on the NR size. As discussed in Refs.[5,49], and as we have explained above, a difference in the plasmon linewidths also leads to induced transparency as a result of Fano interference between the two plasmon modes.

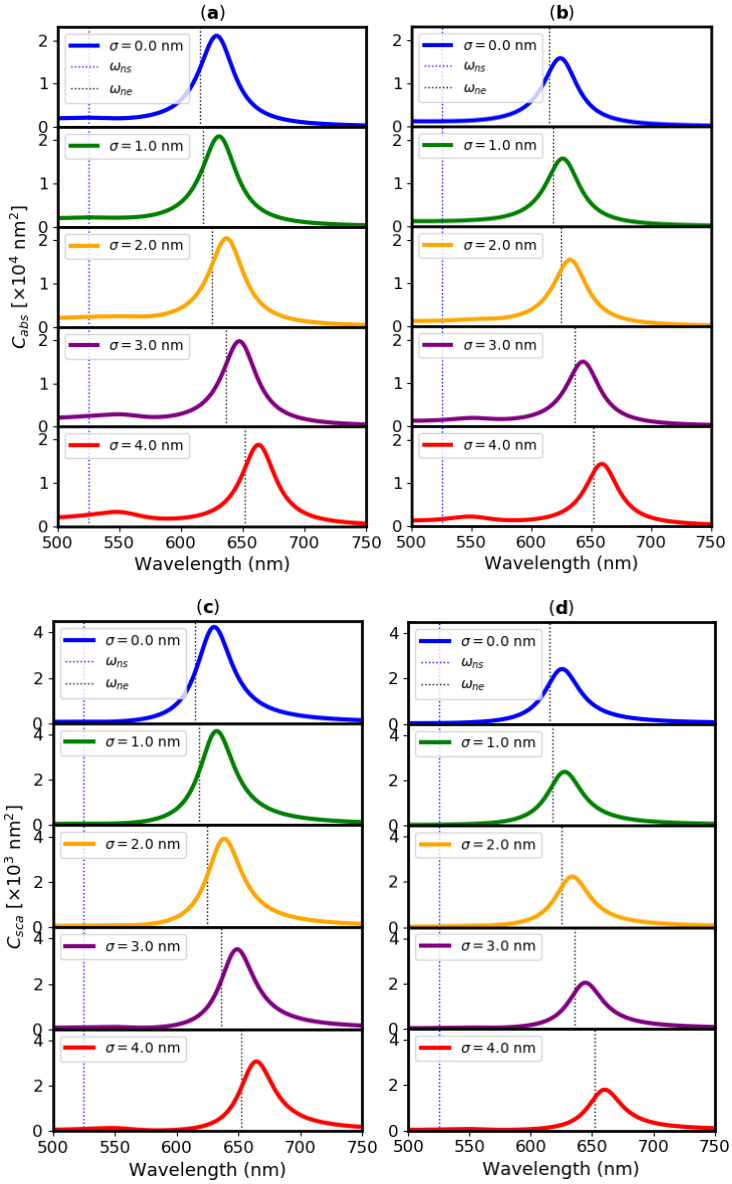

FIG. 5. Absorption cross-sections of the NE-NS dimer (top row, (**a**) and (**b**)), and scattering cross-sections of the NE-NS dimer (bottom row, (**c**) and (**d**)), respectively, for the different core-offsets of the NE, in the case of nanospheres with the same volume as the blueshifted nanorods: (**a**) and (**c**) (24 nm, 12 nm) NR, r = 15.12 nm, and (**b**) and (**d**) (15 nm, 6 nm) NR, r = 9.45 nm. The dotted lines represent the plasmon peak positions of the NS and NE, respectively.

Plasmon coupling in the NE-NR dimer depends on both the plasmon detuning frequency and the NR size. The appearance of transparency dips in the dimer spectra for all NR spectral peak positions studied shows that for a given NE size, the dimer can be strongly coupled depending on the detuning frequency and the NR size. The latter determines the plasmon coupling strength through the half-length of the NR[52] and Fano interference through the NR absorption linewidth[7], while

the former determines plasmon hybridization. This is consistent with plasmon coupling in other heterodimers[7,29] where plasmon-induced transparency has been reported.

In addition, the redshifts in the hybrid plasmon modes of the NE-NR dimer and the enhanced spectra of the dimer (Figs. 3 and 4) are consistent with the trends reported in Ref.[29] for an incident field parallel to the dimer axis. However, the NE-NR heterodimer is such that decreasing or increasing the detuning frequency at constant NE size can lead to induced transparency, depending on the spectral peak position of the NR. In addition, a small NR whose absorption cross-section is less than that of the NE at a redshifted plasmon peak position tends to induce more transparency dips in the dimer spectra, irrespective of the detuning frequency, compared to a small NR with similar absorption cross-section at a blueshifted or resonant plasmon peak position. This might be related to the direction of the core-offset, which is towards the NR in the redshifted NR case. However, in comparison to the NS-NR dimer studied in Ref.[7], it could also be due to both the redshifted spectral peak position of the NR and the positioning of the NE along the NR long axis.

Both the absorption and scattering spectra of the NE-NR dimer show a common trend: the emergence of mode splittings and plasmon-induced transparency dips as the detuning frequency is tuned via the core-offset of the NE at a constant NR size, in addition to plasmon-induced LSPR shifts. However, similar to the spectral behaviour of the NR dimer studied in Ref.[49], the scattering dips are greater than the absorption dips due to their different dependence on the wavelength of light in the medium. For instance, compared to the absorption spectra in Fig. 3(**f**), the scattering spectra of the redshifted NR case in Fig. 4(**f**) are almost entirely transparent between 630 nm and 670 nm.

B. Plasmon-Induced LSPR Shifts

Due to plasmon coupling, ω_{ne} and ω_{nr} undergo plasmon hybridization to form new dipolar plasmon modes. Depending on the detuning frequency and the NR size, both plasmon-induced transparency and plasmon-induced LSPR shift will occur or only the latter occurs in the dimer spectra. The spectral peak positions of the NE-NR dimer (Fig. 3) correspond to the plasmon resonances of these new modes. As summarized in Table I for the small nanorods with $d = 15$ nm, the hybrid plasmon modes of the dimer inherit the intrinsic property of the NE, i.e., they undergo a redshift with increasing core-offset, depending on whether the NR absorption leads to mode splitting in the dimer spectra. A redshift is also expected for an incident field parallel to the dimer axis[28,29]. However, the sensitivities of the hybrid plasmon modes to changes in the core-offset differ due to the different NR polarizabilities.

In Fig. 6, the scattering cross-section of the dimer is significantly enhanced in the blueshifted NR case (Fig. 6(**a**)), due to a longer half-width of the NR, compared to the other cases (Fig. 6(**b**) and (**c**)). When the NR absorption does not lead to a significant induced transparency, the cross-sections of the NE-NR dimer are more enhanced (Fig. 6(**a**) and (**b**)) compared to the redshifted NR

case (Fig. 6(**c**)). Plasmon coupling leads to a strong redshift in ω_{ne} to form a bright, low-energy hybrid plasmon mode, ω_-, whose scattering intensity decreases with increasing core-offset (Fig. 6(**a**)), compared to Fig. 6(**b**) and (**c**), where the intensity of the bright hybrid mode increases with increasing core-offset. However, in the latter two cases, the intensity of the bright mode is affected by induced transparency in the scattering spectra of the dimer since the NR absorption is reduced further compared to that of the NE. A new, weak, high-energy hybrid plasmon mode, ω_+, is then formed, depending on the plasmon detuning frequency. For the small nanorods, only ω_- is formed in the blueshifted NR case, as shown in Fig. 6(a) and in Table I. In the dispersion curves in Fig. 6(**b**) and (**c**), the weak scattering peak is hardly visible in the redshifted NR case (Fig. 6(**c**)), while it is completely absent in the resonant NR case (Fig. 6(**b**)). For the redshifted NR, ω_+ vanishes gradually as the core-offset is increased (Fig. 4(**f**)), due to a decrease in the detuning frequency. Depending on the spectral peak position of the NR and its size, the respective sensitivity of the hybrid plasmon modes to changes in the core-offset differs, i.e., ω_+ is more sensitive in the redshifted NR case, while ω_- is more sensitive in both the blueshifted and resonant NR cases. Also, ω_+ is formed by a plasmon-induced blueshift in ω_{ne} for the redshifted NR. On the other hand, ω_- is formed by a plasmon-induced redshift in ω_{ne} for the blueshifted and resonant nanorods, while it is due to a redshift in ω_{nr} for the redshifted NR. This is depicted in the energy-level diagram in Fig. 7.

Isolated NE		NE-NR dimer with a blueshifted NR	NE-NR dimer with a resonant NR		NE-NR dimer with a redshifted NR		
		$c = 7.5$ nm	$c = 6.0$ nm		$c = 5.0$ nm		
		$\omega_{nr} = 586$ nm	$\omega_{nr} = 625$ nm		$\omega_{nr} = 673$ nm		
σ (nm)	ω_{ne} (nm)	ω_- (nm)	ω_- (nm)	ω_+ (nm)	ω_- (nm)	ω_+ (nm)	χ (meV)
0	615	635	653	598	692	606	92.835
1	618	638	654	600	693	609	92.225
2	625	642	657	–	695	615	91.980
3	636	651	662	–	697	625	87.340
4	652	665	671	–	699	636	82.700

TABLE I. Dependence of ω_{ne}, ω_-, ω_+, and χ on the core-offset, σ, of the NE, for the small nanorods.

Plasmon coupling in metal nanoparticle dimers has been described previously using a coupled harmonic oscillator (CHO) model[7]. Here, we adopt the same model in order to determine the plasmon coupling strength in the NE-NR dimer when the NR absorption leads to mode splitting for all the core-offsets studied, i.e., for the small redshifted NR. We seek a relationship between the detuning frequency, the coupling strength, and mode splitting. The CHO model gives the hybrid plasmon modes as[47,49,50,56]

$$\omega_\pm = \frac{1}{2}(\omega_{ne}+\omega_{nr}) - \frac{i}{4}(\gamma_{nr}+\gamma_{ne}) \pm \frac{1}{2}\sqrt{4\chi^2 + \left[(\omega_{ne}-\omega_{nr}) + \frac{i}{2}(\gamma_{nr}-\gamma_{ne})\right]^2}, \qquad (28)$$

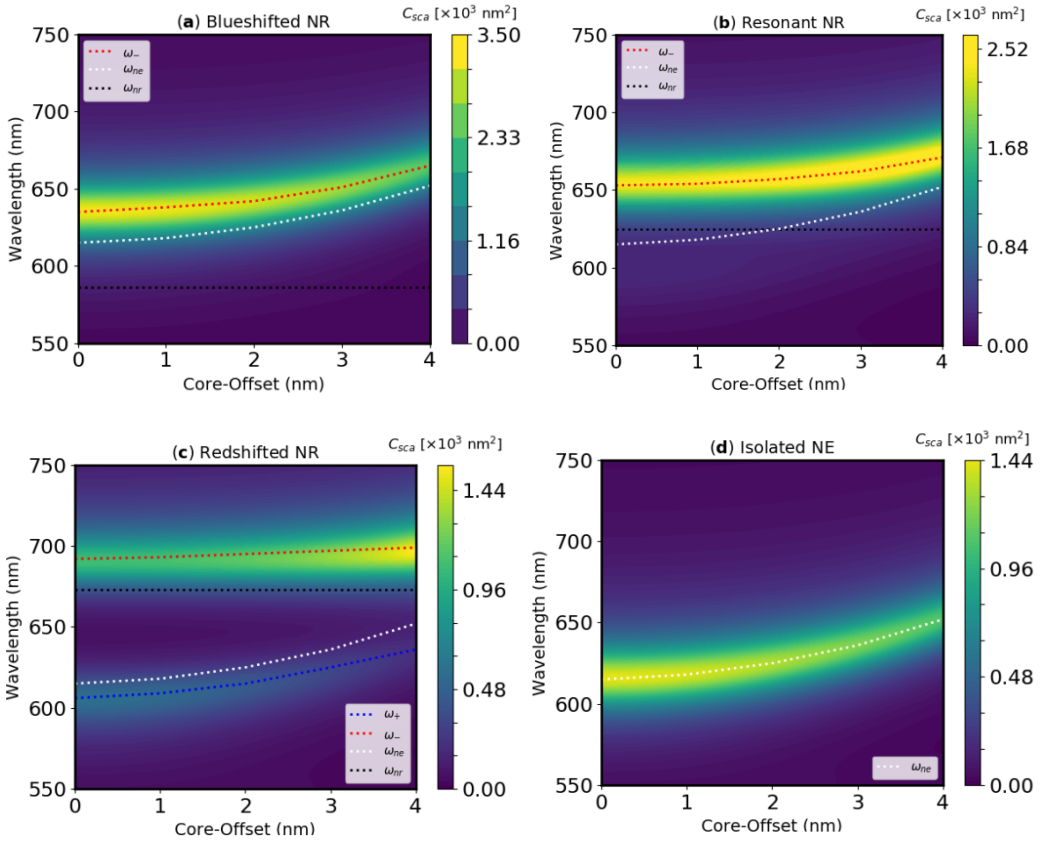

FIG. 6. Contour plots of the scattering cross-sections of the NE-NR dimer, showing the dispersion curves when the NE is coupled to the (**a**) blueshifted, (**b**) resonant, and (**c**) redshifted, small nanorods, with respect to the plasmon peaks of the isolated NE, and (**d**) contour plot of the scattering cross-section of the isolated NE. The colour bars indicate the maximum value of the scattering cross-section in each case. The line plots represent the dependence of ω_{ne}, ω_+ and ω_- on the core-offset, respectively, with respect to ω_{nr}, while the "smearing" around them is due to their imaginary parts, i.e., the plasmon linewidths.

where we have rewritten the equation in terms of the model parameters of the NE-NR dimer. Here, ω_{ne} and ω_{nr} are the LSPR of the NE and NR, respectively, γ_{ne} and γ_{nr} are the dipolar plasmon linewidths of the NE and NR, respectively, χ is the dipole–dipole plasmon coupling strength of the NE-NR dimer, ω_+ is the high-energy hybrid plasmon mode, and ω_- is the low-energy hybrid plasmon mode. In Eq. (28), the $(\omega_{ne}-\omega_{nr})$ term determines whether plasmon hybridization will occur, the $(\gamma_{nr}-\gamma_{ne})$ term determines Fano interference, while a combination of either of these two terms or both, and χ, determines the mode splitting. From Eq. (28), we obtain the coupling strength as

$$\chi = \frac{1}{2}\sqrt{\Omega^2-\Delta^2}, \tag{29}$$

where we have assumed that $\gamma_{ne} \approx \gamma_{nr}$, which is only true when the NR absorption is comparable to that of the NE or when absorption losses due to plasmon damping are negligible[50]. However,

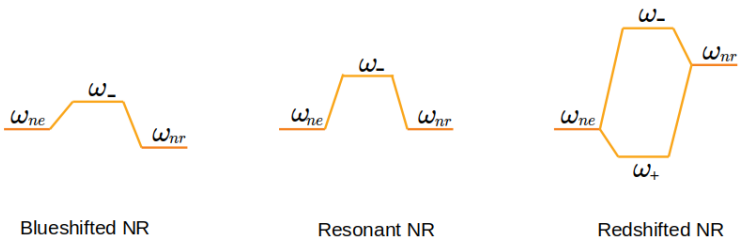

FIG. 7. Plasmon hybridization diagram showing how the spectral peak positions of the small nanorods in Table I and their detuning frequency affect the hybrid plasmon modes and the mode splitting, based on the data for $\sigma = 2.0$ nm.

it allows us to obtain a real χ[49,50]. In Eq. (29), $\Omega = \omega_+ - \omega_-$ is the mode splitting[50,56], and $\Delta = \omega_{ne} - \omega_{nr}$ is the detuning frequency. As shown in Fig. 7, Δ determines ω_-, ω_+, and Ω for a given NR absorption cross-section. For each core-offset, we used Eq. (29) to determine the coupling strengths shown in energy units in Table I. The trends in χ indicate that for a given dimer gap and NR size, the coupling strength decreases gradually with a decrease in the detuning frequency for the redshifted NR. This is also expected since once the NR size is kept constant, only the detuning frequency will determine plasmon-induced transparency in the spectra of the NE-NR dimer.

Ref.[5] has shown that the amplitude of the dipolar mode of a NE decreases with increasing core-offset, due to dipole–quadrupole plasmon coupling. The downside of this plasmonic behaviour is that the absorption and scattering cross-sections of the NE decrease with increasing core-offset, as we have shown in Fig. 2(**a**). However, by coupling the NE to a NR, the absorption and scattering cross-sections of the NE-NR dimer are significantly enhanced, as shown in Figs. 3 and 4, respectively. In addition, the PIT regions in the dimer spectra can be used as a sensing parameter in LSPR spectroscopy to distinguish between NR sizes, since the PIT phenomenon in the dimer is very sensitive to changes in the NR size.

IV. CONCLUSION

We have studied the effect of dipole–dipole plasmon coupling on the scattering and absorption cross-sections of a NE-NR heterodimer. The dimer consists of a silica core–gold shell NE and a gold NR. By using a dipolar quasi-static approach, and considering only the case of an incident electric field parallel to the dimer axis, at constant NE size, we found that plasmon coupling in the NE-NR dimer is dependent on both the absorption cross-section of the NR and the plasmon detuning frequency. This is regardless of whether the NR is at a blueshifted, resonant, or redshifted plasmon peak position with respect to the plasmon peaks of the NE.

When the parameters in the plasmon coupling terms — the NR and NE sizes, their non-interacting polarizabilities, and the dimer gap — are kept constant, plasmon-induced transparency and mode

splitting occur in both the absorption and scattering cross-sections of the dimer as the detuning frequency is tuned via the core-offset of the NE. However, the plasmon-induced LSPR shifts increase slightly with increasing NR size.

In all NR sizes and plasmon peak positions studied, the absorption and scattering spectra of the dimer are enhanced compared to the spectra of the non-interacting NE or NR, respectively. However, larger nanorods lead to more enhanced spectra due to their large polarizabilities. Compared to a NE-NS dimer, the NE-NR dimer features more enhanced spectra but the trends that lead to induced transparency are similar in both dimers.

Funding. L. C. U. was sponsored by the National Research Foundation (NRF) and the University of Pretoria. T. M. was supported by the Czech Science Foundation (GACR) grant no. 18-18022S. T. P. J. K. was supported by the NRF grant nos. N01564 (project 109302) and N00500 (project 120387).

Disclosures. The authors declare no conflicts of interest.

[1]H. Wang, Y. Wu, B. Lassiter, C. L. Nehl, J. H. Hafner, P. Nordlander, and N. J. Halas, "Symmetry breaking in individual plasmonic nanoparticles," PNAS **103**, 10856–10850 (2006).

[2]Y. Wu and P. Nordlander, "Plasmon hybridization in nanoshells with a nonconcentric core," J. Chem. Phys. **12**, 124708 (2006).

[3]M. W. Knight and N. J. Halas, "Nanoshells to nanoeggs to nanocups: optical properties of reduced symmetry core-shell nanoparticles beyond the quasistatic limit," New J. Phys. **10**, 105006 (2008).

[4]J. Zhang and A. Zayats, "Multiple Fano resonances in single-layer nonconcentric core-shell nanostructures," Optics Express **21**, 8426–8436 (2013).

[5]S. J. Norton and T. Vo-Dinh, "Optical Fano resonances in a nonconcentric nanoshell," Appl. Opt. **10**, 2611–2618 (2016).

[6]V. Krivenkov, S. Goncharov, I. Nabiev, and Y. P. Rakovich, "Induced transparency in plasmon-exciton nanostructures for sensing applications," Laser Photonics Rev. **13**, 1800176 (2019).

[7]L. Shao, C. Fang, H. Chen, Y. C. Man, J. Wang, and H.-Q. Lin, "Distinct plasmonic manifestation on gold nanorods induced by the spatial perturbation of small gold nanospheres," Nano Lett. **12**, 14241430 (2012).

[8]S. Link and M. A. El-Sayed, "Shape and size dependence of radiative, non-radiative and photothermal properties of gold nanocrystals," Int. Reviews in Physical Chemistry **19**, 409–453 (2000).

[9]C. F. Bohren and D. R. Huffman, *Absorption and scattering of light by small particles* (John Wiley and Sons, Inc., 2008).

[10]A. Mohammadi, V. Sandoghdar, and M. Agio, "Gold nanorods and nanospheroids for enhancing optical emission," New J. Phys. **10**, 105015 (2008).

[11]V. Myroshnychenko, J. Rodrguez-Fernández, I. Pastoriza-Santos, A. M. Funston, C. Novo, P. Mulvaney, and F. J. G. de Abajo, "Modelling the optical response of gold nanoparticles," Chemical Society Reviews **37**, 1792–1805 (2008).

[12]A. Moroz, "Depolarization field of spheroidal particles," J. Opt. Soc. Am. B **26**, 517–527 (2009).

[13]J. Zuloaga, E. Prodan, and P. Nordlander, "Quantum plasmonics: optical properties and tunability of metallic nanorods." ACS nano **4**, 5269–5276 (2010).

[14]M. Yorulmaz, S. Khatua, P. Zijlstra, A. Gaiduk, and M. Orrit, "Luminescence quantum yield of single gold nanorods," Nano Lett. **12**, 4385–4391 (2012).

[15]S. L. Smitha, K. G. Gopchandran, N. Smijesh, and R. Philip, "Size-dependent optical properties of Au nanorods," Progress in Natural Science: Materials International **23**, 3643 (2013).

[16]Y.-F. Chau, M. W. Chen, and D. P. Tsai, "Three-dimensional analysis of surface plasmon resonance modes on a gold nanorod," Appl. Opt. **48**, 617–622 (2009).

[17]Y.-F. C. Chau, C. M. Lim, C. Lee, H. J. Huang, C.-T. Lin, N. T. R. N. Kumara, V. N. Yoong, and H.-P. Chiang, "Tailoring surface plasmon resonance and dipole cavity plasmon modes of scattering cross section spectra on the single solid-gold/gold-shell nanorod," J. Appl. Phys. **120**, 093110 (2016).

[18]L. C. Ugwuoke, T. Mančal, and T. P. J. Kruger, "Localized surface plasmon resonances of simple tunable plasmonic nanostructures," Plasmonics **15**, 189–200 (2020).

[19]R. Esteban, A. G. Borisov, P. Nordlander, and J. Aizpurua, "Bridging quantum and classical plasmonics with a quantum-corrected model," Nature Communications **3**, 825 (2012).

[20]P. Nordlander, C. Oubre, E. Prodan, K. Li, and M. I. Stockman, "Plasmon hybridization in nanoparticle dimers," Nano Lett. **4**, 899–903 (2004).

[21]B. Khlebtsov, A. Melnikov, V. Zharov, and N. Khlebtsov, "Absorption and scattering of light by a dimer of metal nanospheres: comparison of dipole and multipole approaches," Nanotechnology **17**, 1437–1445 (2006).

[22]I. Romero, J. Aizpurua, G. W. Bryant, and F. J. G. de Abajo, "Plasmons in nearly touching metallic nanoparticles: singular response in the limit of touching dimers," Optics Express **14**, 9988–9999 (2006).

[23]T. J. Davis, D. E. Gómez, and K. C. Vernon, "Simple model for the hybridization of surface plasmon resonances in metallic nanoparticles," Nano Letters **10**, 2618–2625 (2010).

[24]P. Pramod and K. G. Thomas, "Plasmon coupling in dimers of Au nanorods," Adv. Mater. **20**, 4300–4305 (2008).

[25]P. K. Jain, S. Eustis, and M. A. El-Sayed, "Plasmon coupling in nanorod assemblies: Optical absorption, discrete dipole approximation simulation, and exciton-coupling model," J. Phys. Chem. B **110**, 18243–18253 (2006).

[26]C. G. Khoury, S. J. Norton, and T. Vo-Dinh, "Plasmonics of 3-d nanoshell dimers using multipole expansion and finite element method," Nano Letters **3**, 2776–2788 (2009).

[27]J.-W. Liaw, J.-H. Cheng, C.-S. Chen, and M.-K. Kuo, "Purcell effect of nanoshell dimer on single molecule's fluorescence," Optics Express **17**, 13532 (2009).

[28]L. V. Brown, H. Sobhani, J. B. Lassiter, P. Nordlander, and N. J. Halas, "Heterodimers: Plasmonic properties of mismatched nanoparticle pairs," ACS Nano. **4**, 819–832 (2010).

[29]A. Lombardi, M. P. Grzelczak, A. Crut, P. Maioli, I. Pastoriza-Santos, L. M. Liz-Marzn, N. D. Fatti, and F. Valle, "Optical response of individual Au-Ag@SiO_2 heterodimers," ACS Nano **7**, 2522–2531 (2013).

[30]Y.-F. C. Chau, J.-C. Jiang, C.-T. C. Chao, H.-P. Chiang, and C. M. Lim, "Manipulating near field enhancement and optical spectrum in a pair-array of the cavity resonance based plasmonic nanoantennas," J. Phys. D: Appl. Phys. **49**, 475102 (2016).

[31]Y.-F. C. Chau, H.-H. Yeh, and D. P. Tsai, "Surface plasmon effects excitation from three-pair arrays of silver-shell nanocylinders," Physics of Plasmas **16**, 022303 (2009).

[32]A. Moradi, "Plasmon hybridization in parallel nano-wire systems," Physics of Plasmas **18**, 064508 (2011).

[33]A. Aubry, D. Y. Lei, S. A. Maier, and J. B. Pendry, "Conformal transformation applied to plasmonics beyond the quasistatic limit," Phys. Rev. B **82**, 205109 (2010).

[34]I. Kaminska, J. Bohlen, S. Mackowski, P. Tinnefeld, and G. P. Acuna, "Strong plasmonic enhancement of a single peridinin-chlorophyll a-protein complex on DNA origami-based optical antennas," ACS Nano **12**, 1650–1655 (2018).

[35]L. Xin, M. Lu, S. Both, M. Pfeiffer, M. J. Urban, C. Zhou, H. Yan, T. Weiss, N. Liu, and K. Lindfors, "Watching a single a fluorophore molecule walk into a plasmonic hotspot," ACS Photonics **6**, 985–993 (2019).

[36]S. D. Standridge, G. C. Schatz, and J. T. Hupp, "Distance dependence of plasmon-enhanced photocurrent in dye-sensitized solar cells," J. Am. Chem. Soc. **131**, 8407–8409 (2009).

[37]B. Ding, M. Yang, B. J. Lee, and J. Lee, "Tunable surface plasmons of dielectric core-metal shell particles for dye sensitized solar cells," RSC Advances **3**, 9690–9697 (2013).

[38]Y. Yang, H. B. Gobeze, F. DSouza, R. Jankowiak, and J. Li, "Plasmonic enhancement of biosolar cells employing light-

harvesting complex II incorporated with core-shell metal@tio$_2$ nanoparticles," Adv. Mater. Interfaces **3**, 1600371 (2016).

[39]D. V. Yakimchuk, E. Y. Kaniukov, S. Lepeshov, V. D. Bundyukova, S. E. Demyanov, G. M. Arzumanyanm, N. V. Doroshkevich, K. Z. Mamatkulov, A. Bochmann, M. Presselt, O. Stranik, S. A. Khubezhov, A. E. Krasnok, A. Alu, and V. A. Sivakov, "Self-organized spatially separated silver 3D dendrites as efficient plasmonic nanostructures for surface-enhanced Raman spectroscopy applications," J. Appl. Phys. **126**, 233105 (2019).

[40]J. Gersten and A. Nitzan, "Spectroscopic properties of molecules interacting with small dielectric particles," J. Chem. Phys. **75**, 1139 (1981).

[41]R. Bardhan, N. K. Grady, J. R. Cole, A. Joshi, and N. J. Halas, "Fluorescence enhancement by Au nanostructures: nanoshells and nanorods," ACS Nano **3**, 744–752 (2009).

[42]S. Khatua, P. M. R. Paulo, A. G. H. Yuan, P. Zijlstra, and M. Orrit, "Resonant plasmonic enhancement of single-molecule fluorescence by individual gold nanorods," ACS Nano **8**, 4440–4449 (2014).

[43]Q. Wei, G. Acuna, S. Kim, C. Vietz, D. Tseng, J. Chae, D. Shir, W. Luo, P. Tinnefeld, and A. Ozcan, "Plasmonics enhanced smartphone fluorescence microscopy," Sci. Rep. **7**, 2124 (2017).

[44]F. Kyeyune, J. L. Botha, B. van Heerden, P. Malý, R. van Grondelle, M. Diale, and T. P. J. Kruger, "Strong plasmonic fluorescence enhancement of individual plant light-harvesting complexes," Nanoscale **11**, 15139–15146 (2019).

[45]L. C. Ugwuoke, T. Mančal, and T. P. J. Kruger, "Plasmonic quantum yield enhancement of a single molecule near a nanoegg," J. Appl. Phys. **127**, 203103 (2020).

[46]N. Muhammad, Z. Ouyang, Z.-L. Deng, A. D. Khan, Q. Liu, and X. Tang, "Sensitive label-free sensor with high figure of merit based on plasmonic metasurface with unit cell of double two-split nanorings," J. Mater. Sci. **54**, 6301–6309 (2019).

[47]N. Liu, L. Langguth, T. Weiss, J. Kstel, M. Fleischhauer, T. Pfau, and H. Giessen, "Plasmonic analogue of electromagnetically induced transparency at the Drude damping limit," Nat. Mater. **8**, 158–762 (2009).

[48]J. B. Khurgin, "Slow light in various media: a tutorial," Advances in Optics and Photonics **2**, 287–318 (2010).

[49]X. Wu, S. K. Gray, and M. Pelton, "Quantum-dot-induced transparency in a nanoscale plasmonic resonator," Optics Express **18**, 23633–23645 (2010).

[50]C. Tserkezis, M. Wubs, and N. A. Mortensen, "Robustness of Rabi splitting under nonlocal corrections in plexcitonics," ACS Photonics **5**, 133–142 (2018).

[51]T. Mančal, "Excitation energy transfer in a classical analogue of photosynthetic antennae," J. Phys. Chem. B **117**, 11282 (2013).

[52]M.-T. Cheng, S.-D. Liu, H.-J. Zhou, Z.-H. Hao, and Q.-Q. Wang, "Coherent exciton-plasmon interaction in the hybrid semiconductor quantum dot and metal nanoparticle complex," Optics Letters **32**, 2125–2127 (2007).

[53]S. Campione, L. K. Warne, and L. I. Basilio, "Dipole approximation to predict the resonances of dimers composed of dielectric resonators for directional emission," Radio Science **52**, 1235–1241 (2017).

[54]M. J. Caola, "Solid harmonics and their addition theorems," J. Phys. A: Math. Gen. **11**, L23–L26 (1978).

[55]A. Vial, A.-S. Grimault, D. Macas, D. Barchiesi, and M. L. Chapelle, "Improved analytical fit of gold dispersion: Application to the modeling of extinction spectra with a finite-difference time-domain method," Phys. Rev. **71**, 085416 (2005).

[56]L. Novotny, "Strong coupling, energy splitting, and level crossings: A classical perspective," Am. J. Phys. **78**, 1199–1202 (2010).